Received: 19 December 2022 | Revised: 14 September 2023 | Accepted: 6 October 2023

DOI: 10.1002/mp.16793

RESEARCH ARTICLE

MEDICAL PHYSICS

Development and benchmarking of a dose rate engine for raster-scanned FLASH helium ions

Luisa Rank[1,2] | **Ozan Dogan**[1,3] | **Benedikt Kopp**[1] | **Stewart Mein**[1,4,5,6] | **Gianluca Verona-Rinati**[7] | **Rafael Kranzer**[8,9] | **Marco Marinelli**[7] | **Andrea Mairani**[1,4,5,6,10] | **Thomas Tessonnier**[1,4,6]

[1]Department of Radiation Oncology, Heidelberg Ion-Beam Therapy Center (HIT), Heidelberg University Hospital, Heidelberg, Germany

[2]Faculty of Physics, Karlsruhe Institute of Technology (KIT), Karlsruhe, Germany

[3]Faculty of Physics and Astronomy, Heidelberg University, Heidelberg, Germany

[4]Clinical Cooperation Unit Translational Radiation Oncology, German Cancer Consortium (DKTK) Core-Center Heidelberg, National Center for Tumor Diseases (NCT), Heidelberg University Hospital (UKHD) and German Cancer Research Center (DKFZ), Heidelberg, Germany

[5]Division of Molecular and Translational Radiation Oncology, Heidelberg Faculty of Medicine (MFHD) and Department of Radiation Oncology, Heidelberg University Hospital (UKHD), Heidelberg, Germany

[6]Heidelberg Institute of Radiation Oncology (HIRO), National Center for Radiation Oncology (NCRO), Heidelberg University Hospital (UKHD), Heidelberg Faculty of Medicine (MFHD) and German Cancer Research Center (DKFZ), Heidelberg, Germany

[7]Industrial Engineering Department, University of Rome "Tor Vergata", Rome, Italy

[8]PTW-Freiburg, Freiburg, Germany

[9]Medical Campus Pius Hospital, University Clinic for Medical Radiation Physics, Carl von Ossietzky University Oldenburg, Freiburg, Germany

[10]Medical Physics, National Centre of Oncological Hadrontherapy (CNAO), Pavia, Italy

Correspondence
Andrea Mairani, Thomas Tessonnier.
Heidelberg Ion-Beam Therapy Center (HIT), Department of Radiation Oncology, Heidelberg University Hospital, Heidelberg, Germany.
Email:
Andrea.Mairani@med.uni-heidelberg.de;
Thomas.Tessonnier@med.uni-heidelberg.de

Funding information
National Science Foundation, Grant/Award Number: 1P01CA257904-01A1; EMPIR programme

Abstract

Background: Radiotherapy with charged particles at high dose and ultra-high dose rate (uHDR) is a promising technique to further increase the therapeutic index of patient treatments. Dose rate is a key quantity to predict the so-called FLASH effect at uHDR settings. However, recent works introduced varying calculation models to report dose rate, which is susceptible to the delivery method, scanning path (in active beam delivery) and beam intensity.

Purpose: This work introduces an analytical dose rate calculation engine for raster scanned charged particle beams that is able to predict dose rate from the irradiation plan and recorded beam intensity. The importance of standardized dose rate calculation methods is explored here.

Methods: Dose is obtained with an analytical pencil beam algorithm, using pre-calculated databases for integrated depth dose distributions and lateral penumbra. Dose rate is then calculated by combining dose information with the respective particle fluence (i.e., time information) using three dose-rate-calculation models (mean, instantaneous, and threshold-based). Dose rate predictions for all three models are compared to uHDR helium ion beam (145.7 MeV/u, range in water of approximatively 14.6 cm) measurements performed

Andrea Mairani and Thomas Tessonnier contributed equally to the manuscript.

at the Heidelberg Ion Beam Therapy Center (HIT) with a diamond-detector prototype. Three scanning patterns (scanned or snake-like) and four field sizes are used to investigate the dose rate differences.

Results: Dose rate measurements were in good agreement with in-silico generated distributions using the here introduced engine. Relative differences in dose rate were below 10% for varying depths in water, from 2.3 to 14.8 cm, as well as laterally in a near Bragg peak area. In the entrance channel of the helium ion beam, dose rates were predicted within 7% on average for varying irradiated field sizes and scanning patterns. Large differences in absolute dose rate values were observed for varying calculation methods. For raster-scanned irradiations, the deviation between mean and threshold-based dose rate at the investigated point was found to increase with the field size up to 63% for a 10 mm × 10 mm field, while no significant differences were observed for snake-like scanning paths.

Conclusions: This work introduces the first dose rate calculation engine benchmarked to instantaneous dose rate, enabling dose rate predictions for physical and biophysical experiments. Dose rate is greatly affected by varying particle fluence, scanning path, and calculation method, highlighting the need for a consensus among the FLASH community on how to calculate and report dose rate in the future. The here introduced engine could help provide the necessary details for the analysis of the sparing effect and uHDR conditions.

KEYWORDS
engine, flash, helium ions, radiotherapy, ultra high dose rate

1 | INTRODUCTION

Radiation therapy as cancer treatment aims to maximize the biological effect of radiation to tumor cells while sparing surrounding healthy tissue. Among the therapeutic options, charged particle therapy (CPT) can provide additional normal tissue sparing compared to conventional photon-based radiation therapy due to its conformal dose delivery.[1] In the last years, the radiation therapy community has been highly focused on a novel approach to potentially increase normal tissue sparing while maintaining a similar tumor control: the FLASH effect.[2,3,4] The FLASH effect has been observed for irradiation at high dose per fraction (~10 Gy) with ultra-high dose rate (uHDR), that is, uHDR > 40 Gy/s, with either electrons, photons or heavy charged particle beams.[5–9]

Mean dose rate (trivially dividing total dose by the total irradiation time) is a first-order approximation for FLASH modelling. There are delivery methods using electrons, photons or charged particles, for example, with passive scattering, that achieve a relatively homogeneous dose rate distribution within the irradiation field. However, CPT with pencil beam scanning delivery results in complex spatially variant dose delivery time structures, which limits the validity of the mean dose rate as a general reference quantity.[10,11] To that end, instantaneous dose rate was introduced to describe the local deposition of the dose at one point within the irradiation field during the delivery time. Interplays between the irradiated spots (irradiation pattern) and time lead to a complicated instantaneous dose rate delivery over time for each point within the irradiation field. Thus, for a better understanding of the correlation between the dose rate and the FLASH-sparing effect for CPT with scanned delivery, the impact of the irradiation pattern on the dose rate is crucial as well as a consensus on how the dose rate should be referred to.

Although dose rate (either instantaneous dose rate or mean dose rate) is a key parameter for the FLASH effect, dose calculation engines currently used for in-silico studies do not integrate dose rate for biological calculation of the FLASH sparing. Usually, a fixed dose modification factor is assumed to approximate the FLASH-sparing effect.[12,13] Recently, dose calculation systems were developed that allow for dose rate optimization by changing primarily the spot pattern of the delivery field. However, the instantaneous dose rates from these engines have not been experimentally validated against measurements.[10,11] Furthermore, due to their general availability mostly protons have been used for these studies, while the FLASH effect is investigated for a broad range of ion species.[9,14,15] While most of the FLASH studies are dominated by electron and proton delivery, first investigations on a sparing effect for uHDR helium and carbon ions were reported at the Heidelberg Ion-Beam Therapy Center (HIT) with raster-scanned delivery.[9,14]

This work aims to develop a dose rate engine for raster scanned uHDR particle therapy adapted from the independent framework established in-house at HIT: the

FRoG (Fast dose Recalculation on GPU) engine.[16,17] HIT has been at the forefront of bringing helium ions back to clinical practice, after the shutdown of the 184-Inch synchrocyclotron at LBNL. Compared to protons, helium ions provide enhanced dose conformity and higher LET, while showing reduced fragmentation tail compared to carbon ion beams.[18] In 2021, the first patient was treated with active scanning helium ion beams at HITx.[19] Different approaches for dose rate calculation are compared to each other, using in-silico and experimental data.

2 | METHODS

2.1 | Dose and dose rate engine

In this work, the HIT in-house dose engine FRoG has been adapted, allowing dose rate calculation for raster scanned particle therapy. In the following, the two main principles of the calculation engine are summarized.

2.1.1 | Pencil beam algorithm

The dose-calculation engine is based on a pencil beam algorithm.[20] The dose d in a voxel with lateral position (x, y) at a certain depth in water z is determined with

$$d(x,y,z) = \sum_{i=0}^{N} \Phi(\tilde{x}_i - x, \tilde{y}_i - y, z) \cdot \Psi(z),$$

where the sum goes over all N pencil beams at the positions ($\tilde{x}i$,$\tilde{y}i$). Φ describes the lateral beam expansion and Ψ refers to the integrated depth dose distribution.

The depth-dependent lateral beam spread parameters and depth dose distributions are taken from Monte Carlo (MC) derived databases, which have been generated for the FRoG engine. MC simulations have thereby been designed to reproduce the HIT facility commissioning and experimental data. Φ is approximated by a triple-gaussian distribution

$$\Phi\ (x,y,z) = \sum_{i\,=\,0}^{3} w_i \cdot \frac{1}{2\pi\sigma^2_{i,\,tot}\,(z)} \exp\left(-\frac{x^2+y^2}{2\sigma^2_{i,\,tot}\,(z)}\right),$$

where w_i are relative weighting factors and $\sigma_{i,tot}$ is given by

$$\sigma^2_{i,\,tot}\,(z) \;=\; \sigma^2_{init,air} + \sigma^2_{i,water}\,(z)\,.$$

$\sigma_{init,air}$ describes the initial beam shape at the entrance to the target in air and $\sigma_{i,water}(z)$ corresponds to the lateral beam spread in water.[16]

2.1.2 | Implementation of the dose rate engine

The presented engine is designed to calculate as well as analyze temporal and spatial variation in dose rate for experiments at particle therapy facilities. The dose rate engine requires information on the irradiation setup (geometry, position and material) as well as the particle beam plan (particle energy, spot size, spot positions, and number of particles) as summarized in the left panels of Figure 1 (Figure 1(I)–(III)). However, for dose rate calculation, the total particle fluence over the delivery time, measured by the monitoring chambers within the HIT beamline is also required. At HIT, high doses are delivered within a single particle spill to achieve the required uHDR conditions, whereby the duration of one spill is in the order of hundred milliseconds.[15] A representative synchrotron spill measured at HIT with a sampling time of 50 μs is shown in Figure 1-(III). The dose rate engine provides dose and dose rate calculations for any point of interest. Therefore, time-dependent lateral dose and dose rate distributions can be reported as well, as visualized in Figure 1-(VI).

Various definitions of dose rate in the context of uHDR pencil beam scanned irradiation are available in literature. The conservative approach is to report the mean dose rate, which refers to the ratio of the total dose divided through the total irradiation time.[21,22] As illustrated in Figure 1-(IV), most of the dose is applied in a time that is much shorter than the total irradiation time for raster scanned irradiation. Therefore, recent publications propose an adjusted time window to characterize the dose rate for FLASH experiments.[15,23] This is why, in addition to mean dose rate calculations, another dose rate definition was employed,[23] where thresholds are implemented to identify low dose contributions at the beginning and end of the irradiation.

Dose rate calculation is started at time t_0 when a dose threshold value of d† is reached, and stopped at time t_1 when the accumulated dose exceeds D($\vec{r}$)—d†, whereby D($\vec{r}$) refers to the total dose at point $\vec{r}$.[23] Consequently, the dose rate $\dot{d}$ at point $\vec{r}$ is defined as:

$$\dot{d}\ \left(\vec{r}\right) = \frac{D\left(\vec{r}\right)\ -\ 2d\dagger}{T\left(\vec{r}\right)},$$

where $T(\vec{r})$ is the "effective" irradiation time,[23] defined as

$$T\ \left(\vec{r}\right) = \ t_1 - t_0.$$

In this work, d† is set to 5% of the total dose. Hereinafter, dose rate values determined in this manner are referred to as $\dot{d}5{-}95$ values. Figure 1-(IV) and Figure 1-(V) visualize the methodology for determining those values.

To correlate the spatial information of pencil beams with the corresponding beam intensity over time, the

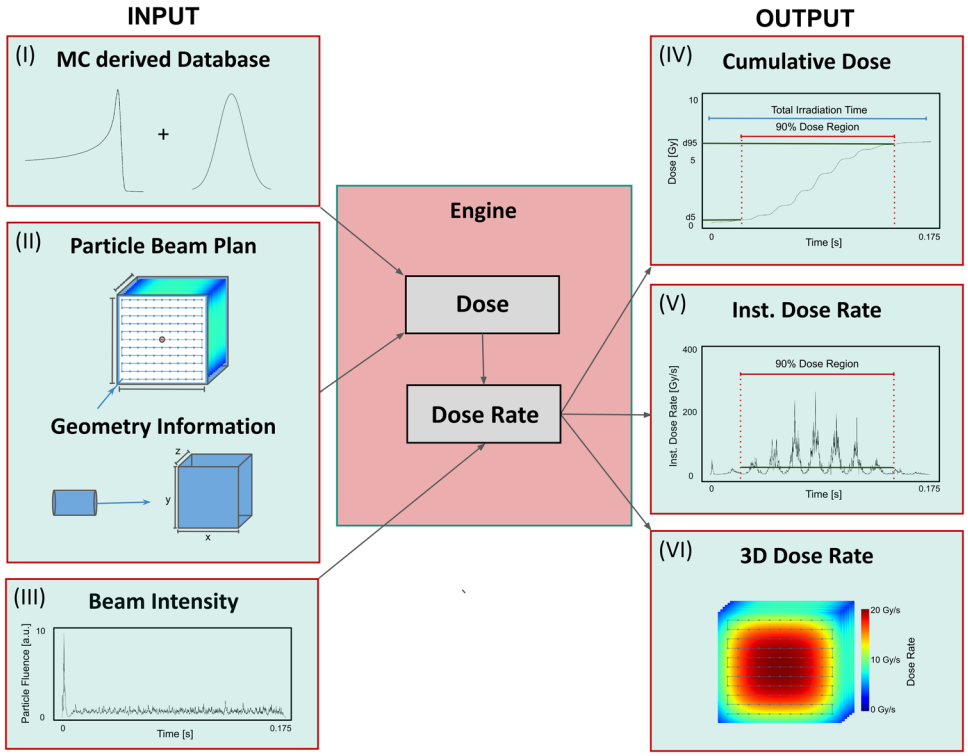

FIGURE 1 Graphical visualization of the simulation code architecture. Panel (I)-(III): Input data needed to perform dose and dose rate calculation; the MC derived database, the particle beam plan, information on the traversed material (geometry information) and information on the particle fluence (beam intensity). Panel (IV)-(VI): Specific dose rate calculation output (dose rate and cumulative dose as well as 3D dose rate distributions). The red bars in the cumulative dose and instantaneous (inst.) dose rate plots indicate the "effective" irradiation time where 90% of the total dose is applied. The green bar in the instantaneous dose rate plot refers to the mean dose rate within the effective irradiation time; the $\dot{d}5{-}95$ value.

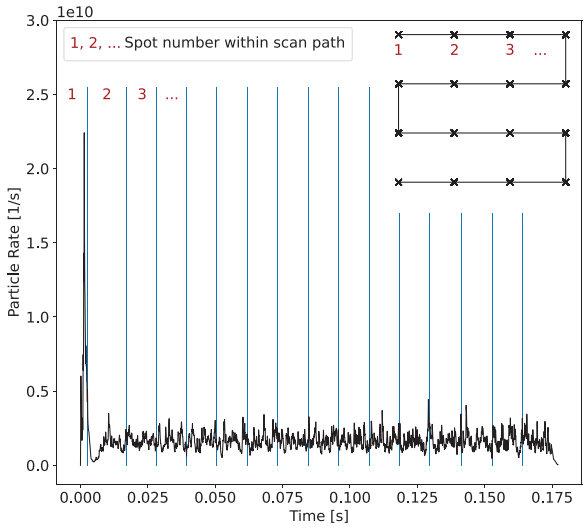

FIGURE 2 Graphical visualization of the particle spill-spot pattern-assignment process. The particle spill is assigned to the spot pattern in order to correlate the spatial information of the pencil beams with the corresponding beam intensity over the time.

recorded particle spill is assigned to the spot pattern after acquisition. Figure 2 illustrates the process in an exemplary manner. For each time frame (in this work 50 μs), the number of particles delivered in this time frame and the beam position is known. The here described pencil beam algorithm can be used to calculate the dose for a specific point within the target. Subsequently, the dose per pencil beam is determined by iteratively feeding the binned information into the algorithm. The total dose to the investigated point as a function of time is determined by cumulatively summing the individual pencil beam contributions. With this approach, time information for every pencil beam exists. By combining dose evolution information with time information from the particle spill structure the instantaneous dose rate, that is, the temporal dose rate evolution, is calculated.

2.2 | Benchmarking

2.2.1 | Experimental setup

The delivery and measurement of dose and dose rate was performed at HIT, following experimental procedure for instantaneous dose rate acquisition.[24] For each investigated plan, the delivery time structure of the irradiated spill was recorded by the beam monitor chamber with a 50 μs time resolution for a helium ion beam irradiation with an energy of 145.7 MeV/u

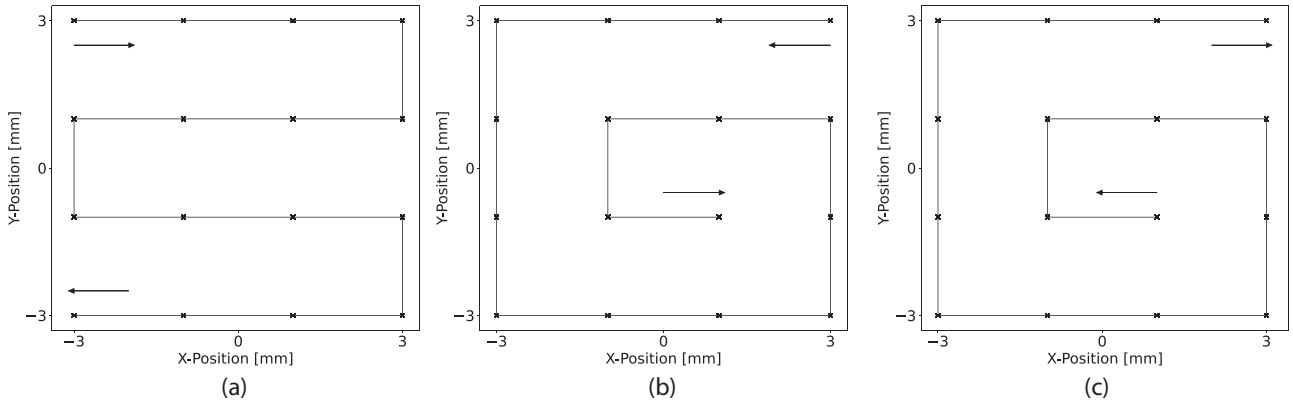

FIGURE 3 Different scanning patterns. Panel (a): Standard raster scanning pattern. Panel (b): Snake-like scanning pattern starting from the outside. Panel (c): Snake-like scanning pattern starting from the inside.

(range in water of approximatively 14.6 cm). Dose rate measurements were performed with diamond prototype detectors (sensitive volume 1.1 mm in diameter, 1 μm thick, PTW) coupled with a transconductance amplifier (DLPCA200-FEMTO) and a digital oscilloscope.[24,25]

To investigate the performance of the dose rate engine in-depth along the beam, a 2 cm $\times$ 2 cm field with a 2 mm spot separation in x and y, resulting in 121 individual spots was used. The number of particles was set to 2.2×10^9, close to the maximum number of particles deliverable in one spill with helium ions at HIT at the time of the study. Consequently, the maximum dose in the Bragg Peak region was about 7.3 Gy for a delivery time of ~180 ms. A standard raster-scanned pattern was used, similar to the pattern displayed in Figure 3a. Measurements were performed in a water tank with its entrance window located 10 cm before the isocenter, with the diamond prototype detector positioned at different water equivalent depths ranging from 2.3 cm to 14.8 cm. Additional lateral measurements for dose rate assessment were acquired in a near Bragg peak region, at 14.5 cm in depths. Six positions were investigated for each direction, from 4.5 to 14.5 mm in X and 3.5 to 13.5 mm in Y, with 2 mm steps.

Furthermore, instantaneous, $\dot{d}5{-}95$ and mean dose rate differences were investigated for different field sizes and delivery patterns. Plans using constant spot spacing (2 mm) with varying square field sizes were used, resulting in plans with 16 spots, 25 spots and 36 spots. The effect of the scanning path was investigated for different patterns, as shown in Figure 3, with: a standard raster scanning pattern, a snake-like scanning pattern starting from the outside and a snake-like scanning pattern starting from the inside. The total number of particles for the 25 and 16 spots plans was set to 2.6×10^9 ions, and to 1.0×10^9 ions for the 36 spots plans. The beam intensity was constant for all plans, resulting in total delivery times of approximatively 160 ms for the 16 and 25 spots plans and 50 ms for the 36 spots plans. The maximum dose at the Bragg peak is about 29.4 Gy for the 16 spots plans, 25.8 Gy for the 25 spots plans and 8.3 Gy for the 36 spots plans. Field size measurements were performed in a RW3 slab (PTW) positioned at the isocenter, with the measurement point at 2 cm water equivalent.

2.2.2 | Analysis

Depth- and lateral dependent dose rate calculations were performed to benchmark the dose rate engine against reference measurements. In accordance with the experimental setup, calculations were done for an investigated point (diamond detector position) in the center of the radiation field for each investigated depth or laterally in the near Bragg peak area.

For all investigated positions, the analytically calculated instantaneous dose rate was evaluated against the corresponding experimentally measured data. As a consequence of the scanned beam delivery, several peak areas can be identified in the dose rate curves. Each peak corresponds to a local minimum in the distance between beam position and investigated point. This means that for a standard raster scanned irradiation each peak can be assigned to one line in the scanning pattern. To assess the calculation performance, the ratio between calculated dose and experimental counterpart within one peak area, hereinafter referred to as dose ratio value, was determined for each investigated depth. The peak areas were identified using thresholds on the instantaneous dose rate, that is, a peak area starts when the instantaneous dose rate exceeds a critical value (threshold) and ends when the instantaneous dose rate falls below that critical value again. To prevent local fluctuations in the instantaneous dose rate curves from being misidentified as peaks, constraints on the time between successive peaks have been implemented. Additionally, mean dose rate and $\dot{d}5{-}95$ values were calculated for 13 depths between 2.3 cm and 14.8 cm and

TABLE 1 Validation of depth-dependency calculations of dose rate with the focus width recorded from the monitoring system.

		Dose Ratio						
	Depth	**Peak 1**	**Peak 2**	**Peak 3**	**Peak 4**	**Peak 5**	**Peak 6**	**Peak 7**
Entrance region	2.3 cm	0.96	0.92	0.95	0.99	1.15		
	4.7 cm	0.98	0.95	0.95	0.96	1.08		
	7.2 cm	1.01	0.96	0.93	0.91	0.99		
	9.2 cm	1.07	0.96	0.97	0.93	1.00		
	11.2 cm	1.08	0.96	0.93	0.90	0.91		
	12.2 cm	1.06	0.98	0.93	0.89	0.92		
	13.2 cm	1.07	1.01	0.94	0.90	0.90		
	13.7 cm	1.10	1.00	0.94	0.88	0.88		
Bragg peak region	14.2 cm	1.32	1.15	1.01	0.93	0.87	0.85	0.83
	14.4 cm	1.23	1.09	1.01	0.94	0.89	0.90	0.90
	14.6 cm	1.24	1.11	1.00	0.92	0.88	0.90	0.86
	14.7 cm	1.30	1.14	1.00	0.95	0.87	0.86	0.89
	14.8 cm	1.21	1.11	1.02	0.95	0.90	0.87	0.82

Note: Dose ratio values for the five highest peaks (entrance region) or seven highest peaks (Bragg peak region) are depicted for all investigated depths.

compared with the corresponding experimental data. Lateral dose rate profiles were simulated in both X and Y and evaluated against the measurement data for the 12 investigated points in near Bragg peak region. The dose rate calculations were performed using the expected focus width taken from the beam plan and an estimated focus width based on data from the monitoring system.

For further verification of the calculation performance under varying particle beam plans and spill structures dose rates were simulated using the beam plan focus width for irradiated plans using RW3 plates. Corresponding to the experimental setup, the depth value was set to 2 cm in the calculations. The impact of varying numbers of irradiated points and scanning patterns on the mean dose rate and $\dot{d}5{-}95$ value was investigated in comparison with experimental data.

The presented simulated dose rates are based on a 50 μs beam intensity record. Therefore, all experimentally measured dose rates were averaged such that the time difference between two successive datapoints matches the simulated counterpart. Furthermore, all instantaneous dose rates are normalized with respect to the total dose.

3 | RESULTS

3.1 | Depth- and lateral-dependent validation

The depth-dependent validation results are shown in Figure 4, Figure 5 and Table 1. As can be seen from Figure 4b-(I), the simulated dose rate curve is in good agreement with experimental data for a representative depth of 14.2 cm. For the beam plan and scanning pattern used (Figure 4a), eleven dose rate maxima occur. Each maximum can be assigned to one line in the scanning pattern (red numbering in Figure 4a). During dose ratio analysis, a subdivision into corresponding peak areas was made. The process is visualized for a depth of 14.2 cm in Figure 4b-(II). Here, for the three highest peaks in the dose rate curves, the simulation deviates from the experimental data by less than 13% with the recorded beam focus width from the monitoring system (about 50% larger than planned). Deviations of about 20% are found when using the planned beam width. Table 1 summarizes the dose ratio values for all investigated depths and peak areas. The mean relative difference between simulations with beam width modification and measurements is 5.6% (11.2% without adapting the beam width) regarding the dose ratio for the three highest peaks in the dose rate curves for all depths investigated.

Figure 4c visualizes the mean dose rate and the $\dot{d}5{-}95$ value for a depth of 14.2 cm. To increase readability, simulated and experimental results are shown separately. As the dose rate curves are normalized to the total dose, the mean dose rates are identical for the upper and lower part of the figure. The analytically calculated $\dot{d}5{-}95$ value matches the experimental data within 4.8%. It is important to notice that for this experimental set-up (irradiation pattern and depth) the $\dot{d}5{-}95$ value is about 54% higher than the mean dose rate. Figure 4d shows the cumulative dose evolution of the experimental measurement and simulations with/without focus width adaptations, highlighting the impact of the initial beam width on the determination of the $\dot{d}5{-}95$ value.

Figure 5 presents experimental and computed $\dot{d}5{-}95$ values in depth and laterally near the Bragg peak. More specifically, figure 5a-(I) shows the computed $\dot{d}5{-}95$

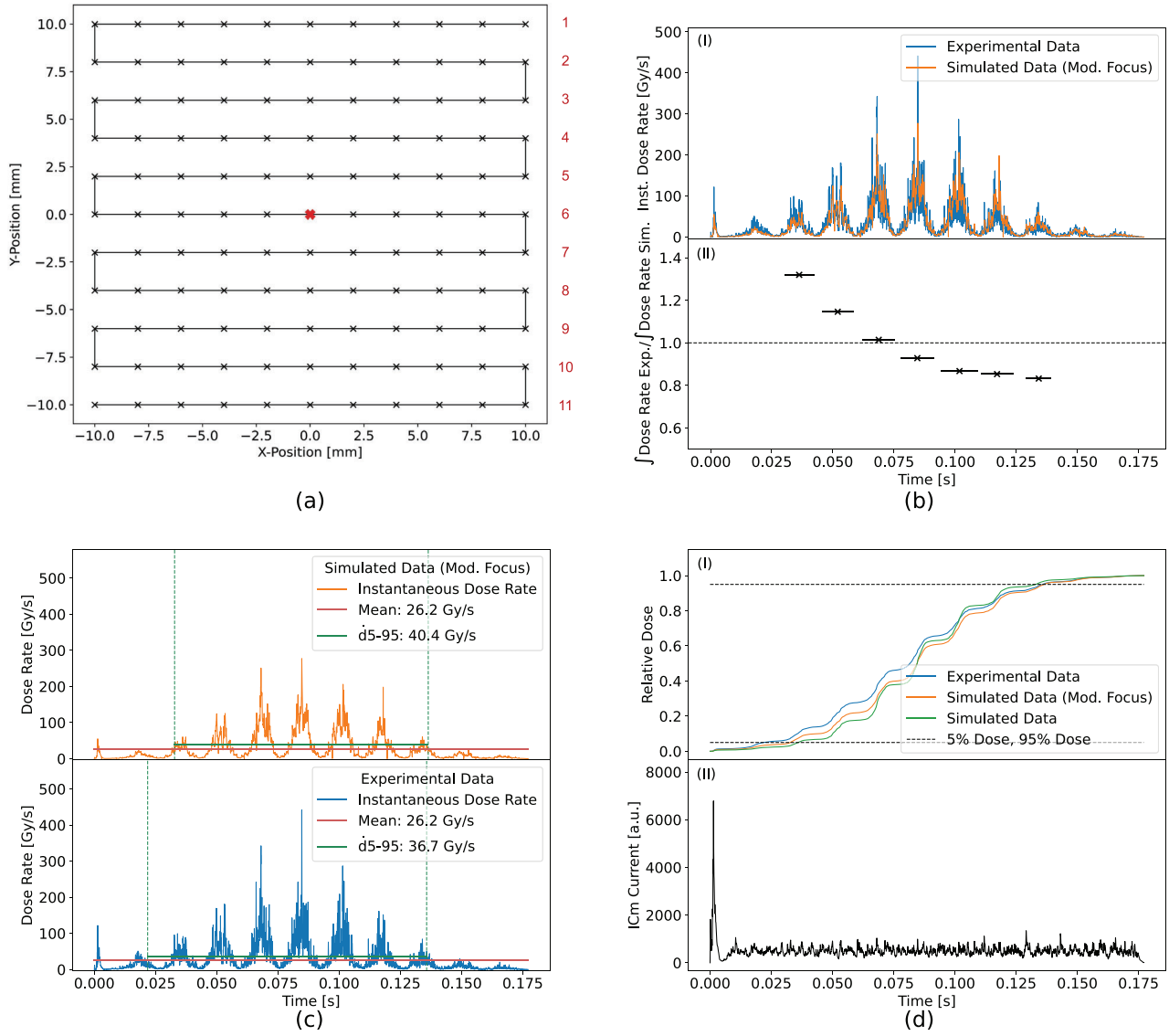

FIGURE 4 Depth dependent validation analysis. Panel (a): Visualization of particle beam plan and scanning pattern. The investigated point within the target is marked with a red cross. Panel (b)-(I): Analytically calculated instantaneous dose rate (with the recorded focus width from the monitoring system) versus experimentally measured dose rate for a representative depth of 14.2 cm. Panel (b)-(II): Ratio between the integrals of the measured and simulated dose rates. The horizontal bars represent the integration interval for each peak. Panel (c): Calculated instantaneous dose rate, displayed for both calculation with the recorded focus width from the monitoring system (upper panel) and measurement (lower panel), together with the respective mean dose rates and $\dot{d}5{-}95$ values. Panel (d)-(I): Cumulative dose evolution as a function of the delivery time for the experimental and simulates dose depositions (with and without modified focus width). The 5% and 95% dose thresholds are depicted with dotted lines. The delivery spill structure for this irradiation can be seen in Panel (d)-(II).

values for all investigated depth values versus the corresponding measurement data. The percental deviation between experiment and calculation ranges between 0.5% and 7.7% as can be seen from Figure 5a-(II). All measurement points in depth passed a 1D gamma-index using a criterium of 5% local dose-rate and 1 mm. Figure 5b-(I) and 5c-(I) show the computed $\dot{d}5{-}95$ values for all investigated lateral positions in X and Y, versus the corresponding measurement data. The percental deviation between experiment and calculation ranges between −1.3% and 3.8% in X, and between −2.5% and 9.4% in Y. All measurement points laterally (in both X and Y) passed a 1D gamma-index using a criterium of 5% local dose-rate and 1 mm.

3.2 | Field size and scanning pattern dependent validation

Figure 6 summarizes the effect of field size and scanning path on the dose rate for measurements and calculations at one point in the irradiation field. Measured

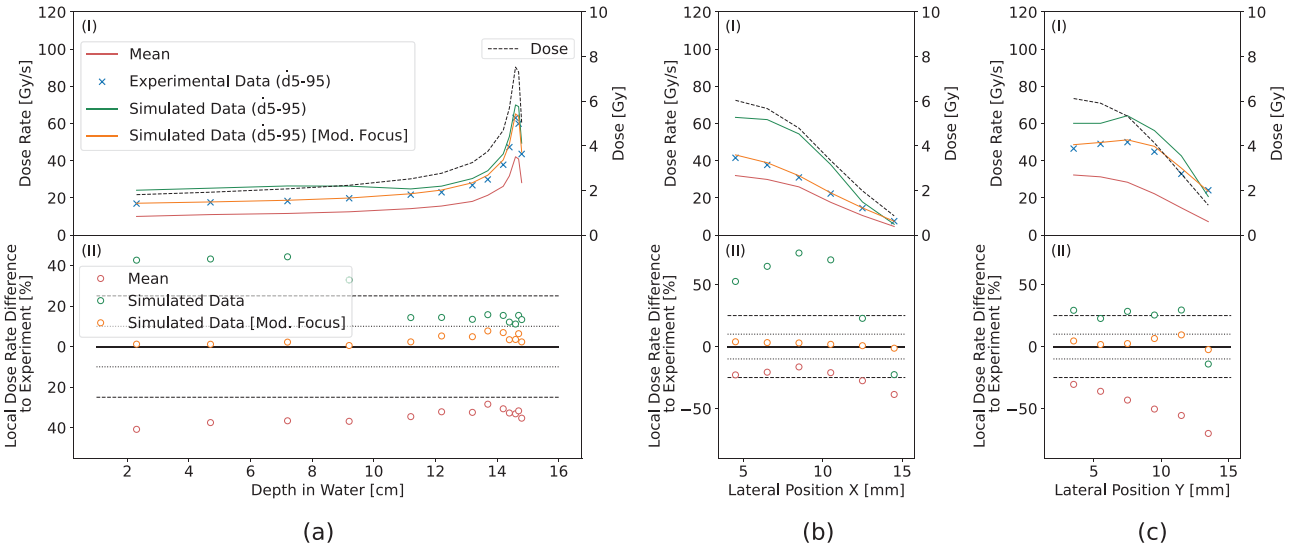

FIGURE 5 Depth and lateral dependent validation results. Panel (a)-(I): Dose (dashed line), mean dose-rate (red), experimentally determined $\dot{d}5{-}95$ values (cross) and calculated $\dot{d}5{-}95$ curve (solid line) without and with modified focus width (green and orange), as a function of depth. Panel (a)-(II): Relative differences between simulated and measured $\dot{d}5{-}95$ values as a function of depth. 10% and 25% difference are depicted with dotted and dashed lines respectively. Panel (b)-(I): Dose, mean dose-rate, experimentally determined $\dot{d}5{-}95$ values and calculated $\dot{d}5{-}95$ curve without and with modified focus width, as a function of lateral X position. Panel (b)-(II): Relative differences between simulated and measured $\dot{d}5{-}95$ values as a function of lateral X position. Panel (c)-(I): Dose, mean dose-rate, experimentally determined $\dot{d}5{-}95$ values and calculated $\dot{d}5{-}95$ curve without and with modified focus width, as a function of lateral Y position. Panel (c)-(II): Relative differences between simulated and measured $\dot{d}5{-}95$ values as a function of lateral Y position.

dose rates versus analytically calculated instantaneous dose rates and respective scanning patterns are shown. The red cross depicts the measurement point. The measured beam intensities, used to calculate the dose rates, are presented underneath the dose rate curves. Additionally, mean dose rate and $\dot{d}5{-}95$ values are displayed in the legend. The simulated dose rate curves are in good agreement with the results from the experimental measurement. Relative differences in the $\dot{d}5{-}95$ values between experiment and simulation range between 0.2% for a snake-like scanned irradiation starting from the inside with 16 beam spots and 29.5% for a standard raster-scanned irradiation with 36 beam spots.

As can be seen from Figure 6, the dose rate amplitude depends on the number of irradiated points, which is linked to the target size, for the same total number of particles. The more irradiated points are considered in the plan, the lower the mean dose rate and $\dot{d}5{-}95$ value are. Moreover, fluctuations in the beam intensity are reflected in the dose rate curves, which is especially noticeable in Figure 6d.

The scanning pattern directly affects the difference between mean dose rate and $\dot{d}5{-}95$ value at the investigated point near the target center. For standard raster scanning patterns, which are axially symmetrical to the horizontal zero-line, the $\dot{d}5{-}95$ value is significantly higher than the mean dose rate, which can be seen in Figure 6a,b,c. For snake-like scanning patterns there is no significant deviation between the mean dose rate and the $\dot{d}5{-}95$ values for the point investigated.

For the investigated point, the relative difference between mean dose rate and $\dot{d}5{-}95$ value was highest for standard raster scanning patterns (31% to 63%) and increases with the field size. For snake style paths differences around 3% were found.

4 | DISCUSSION

The aim of this work was to develop and experimentally verify a tool for rapid calculation and analysis of dose rates for raster-scanned charged particle beams in uHDR applications. Comparison of analytically calculated dose rates with experimental data showed that the developed framework relatively accurately predicts the instantaneous dose rates. As other established dose rate calculation engines for pencil beam scanning proton FLASH experiments are without an extensive instantaneous dose rate validation,[10,11] to the best of the authors knowledge this work presents the first experimentally validated dose calculation engine for uHDR.

The mean percental deviation between measured and calculated $\dot{d}5{-}95$ values over the evaluated depths between entrance and Bragg peak region was 3.6%. The discrepancy varies between 0.5% for a depth value of 9.2 cm (entrance channel) and 7.7% for a depth value of 13.7 cm (Bragg peak region) as displayed in Figure 4d-(II). All dose rate predictions using the beam focus width from the monitoring system are in excellent agreement

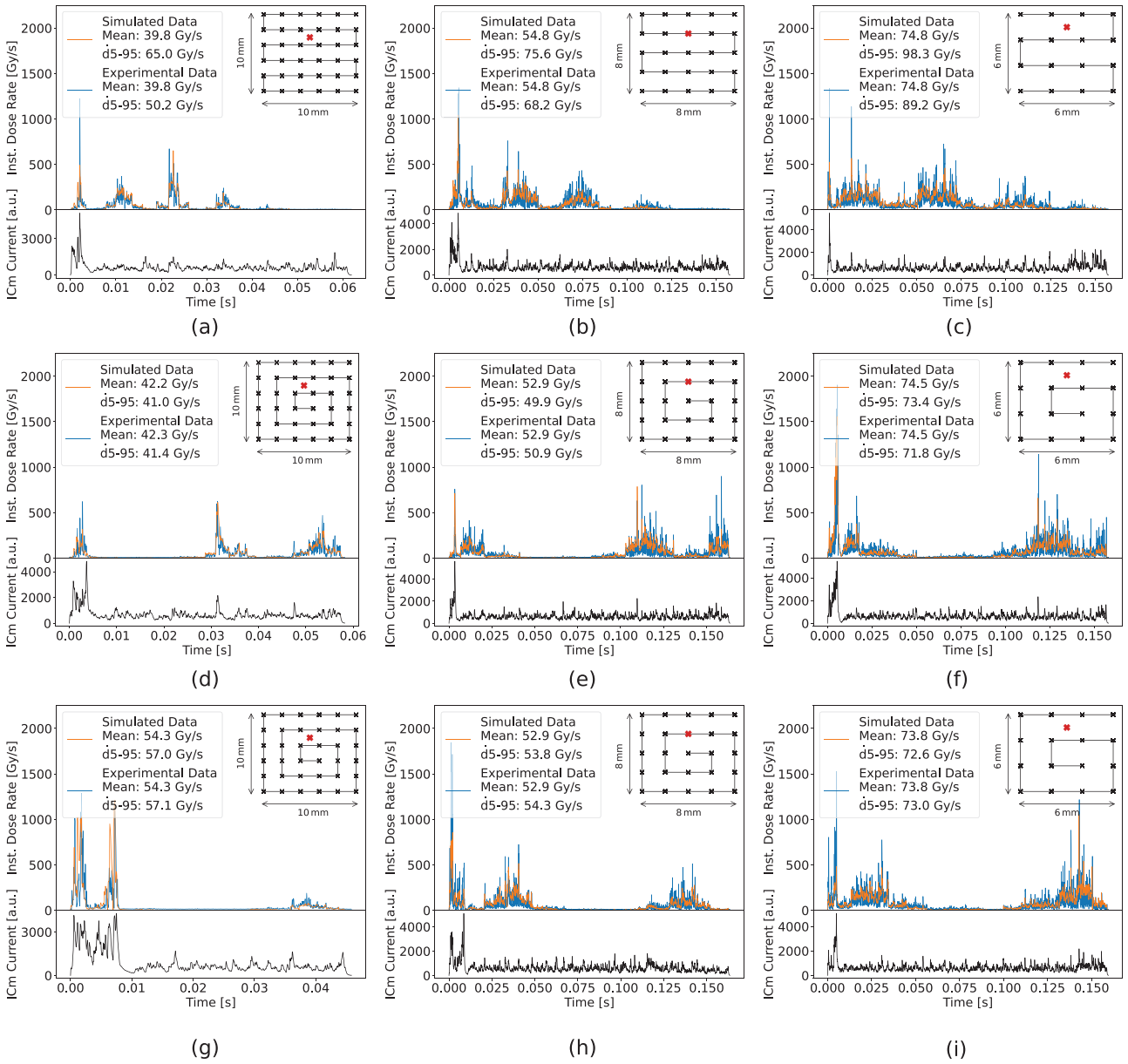

FIGURE 6 Field size and scanning pattern dependent validation results. Analytically calculated instantaneous dose rates versus measured dose rates for different experimental setups are presented. Respective scanning patterns and measured ion chamber currents (ICm Currents) are shown for each figure, whereby the investigated point within the target is marked with a red cross. Panel (a): Irradiation with 36 beam spots and standard raster scanning pattern. Panel (b): Irradiation with 25 beam spots and standard raster scanning pattern. Panel (c): Irradiation with 16 beam spots and standard raster scanning pattern. Panel (d): Irradiation with 36 beam spots and out-in-snake-like scanning pattern. Panel (e): Irradiation with 25 beam spots and out-in-snake-like scanning pattern. Panel (f): Irradiation with 16 beam spots and out-in-snake-like scanning pattern. Panel (g): Irradiation with 36 beam spots and in-out-snake-like scanning pattern. Panel (h): Irradiation with 25 beam spots and in-out-snake-like scanning pattern. Panel (i): Irradiation with 16 beam spots and in-out-snake-like scanning pattern.

with the experimental data both in depth and laterally (1D gamma-index < 1 for a 5% local dose-rate and 1 mm criterium). In contrast to dose measurements where standard protocols[26] are provided, defining the required level of agreement between dose estimation accuracy and dose measurements, for dose rate no such recommendation exists. For carbon ion therapy, biological dose deviations of up to 20%–30% have been observed in a recent study, varying the biophysical model to calculate relative biological effectiveness.[27] The FLASH effect is believed to be a biological response to uHDR depending in part on the magnitude of the dose rate. To that end, with respect to the uncertainties in the biophysical models, 10% dose rate estimation error could be a reasonable threshold, ensuring satisfactory prediction capability of calculation engines.

Even though the deviation between measured and calculated $\dot{d}5-95$ values is well within 10% for the simulations performed without modification of the beam focus width, the corresponding dose ratios show a parabular difference. This parabular shape in ratios can be observed for all depths. The systematic error shapes suggest systematic potential modeling errors in the calculation engine, that were reduced using the recorded beam width instead of the initial planned beam width. Furthermore, analyzing the error shape can provide additional information, since asymmetric shape can indicate potential mispositioning laterally. That the planned beam focus size does not describe the experiment sufficiently might be due to the fact, that the initial beam width is affected by using uHDR accelerator settings. Therefore, a re-evaluation of the FRoG HIT beam focus size library is needed for uHDR calculations with helium ions. Further improvements will be made to tune σ_{init} towards uHDR accelerator settings at HIT (initial focus size and shape, beam divergency), monitoring experimentally the variation and stability of the beam shape. Remaining deviations in Figure 5(b) between the simulated and measured dose rate can be linked to remaining uncertainties on the beam widths assessed from the monitoring system since the measurements are made more than 100 cm before the isocenter and then interpolated to the isocenter.

In the field size and scanning pattern study, percental deviations in dose rate between experiment and simulation for the $\dot{d}5-95$ values were 29.5% (Figure 6a), 10.9% (Figure 6b) and 10.2% (Figure 6c) for a standard raster scanned irradiation with 36, 25, and 16 beam spots, respectively. For the snake-like scanning patterns investigated, the relative discrepancies between experimental and calculated $\dot{d}5-95$ values were below 3% (Figure 6d–i). Although most of the investigated configurations show excellent agreement between simulation and measurement, the discrepancy for the standard raster scanned irradiation with 36 beam spots required further analysis. Similar to the depth dependency study, a systematic change in the beam focus size could explain these results. To that end, the focus width was varied to assess its impact on the simulated dose rate. Recalculation with an increase in $\sigma_{init,air}$ by 20% led to a decrease in the calculated $\dot{d}5-95$ value of 11.2 Gy/s. Therefore, one can assume that the deviation between simulation and measurement for the standard raster scanned irradiation with 36 beam spots is due to an insufficient characterization of the beam focus size. Currently, σ_{init} at the isocenter cannot be expected from beam plan and stable defined beam shape might not be ensured with uHDR accelerator settings.

Dose optimization in clinical routine becomes more demanding. In addition to complex optimization functions, balancing dose to organs at risk with target coverage, plan robustness and for heavy ion therapy biological effectiveness consideration are prevalent. Another layer of complexity could be added by new endpoints such as linear energy transfer and the here investigated dose rate. Dose rate has been proven to play an important role in biological effectiveness in radiation therapy but is hard to model due to its 4D nature.[2,22,28] Regardless of its importance for the FLASH effect, currently used clinical treatment planning systems do not yet use optimization objective functions on dose rate.[12,13] Recent pre-clinical studies addressed dose rate-oriented optimization as a future perspective for FLASH radiotherapy treatment planning.[29–33] Dose rate assessment, depending on the planning strategy (using, e.g., FLASH shoot-trough delivery, FLASH only on the distal energy layer or with beam modifiers) is important in depth and laterally both in the entrance region and in the distal end of the beam.

According to recent publications about uHDR sparing, the mean dose rate may not be the most relevant parameter in the FLASH effect for pencil beam scanning.[15,23,29] As mean dose rate could be influenced by beam pauses or low dose contributions, also the temporal evolution of the dose rate should be considered in the context of FLASH experiments. Therefore, here, a dose rate definition described in previous works, that is, $\dot{d}5-95$ values were investigated.[23]

It was shown that the $\dot{d}5-95$ values are significantly higher than the mean dose rates for particle beam plans with a standard raster scanning pattern, as low dose contributions at the beginning and end of the irradiation time result in reduced average dose rates. For the analytically calculated dataset, shown in Figure 5, the average ratio between mean dose rate and $\dot{d}5-95$ value is 1.57. The absolute deviation varied between 6.8 Gy/s for a mean dose rate of 11.0 Gy/s at a depth value of 4.7 cm and 23.1 Gy/s for a mean dose rate of 42.1 Gy/s at a depth value of 14.6 cm. This highlights the importance and need of accurate dose rate definition and reporting in biological experiments. In addition, the provided comparison between the cumulative dose evolution with and without beam focus adaptation highlight the impact on the beam model on the determination of the $\dot{d}5-95$. Due to the scanning nature of the delivery, the threshold values can have a large impact on the $\dot{d}5-95$ if close to plateau region in the cumulative dose evolution. Furthermore, the impact will be different depending the field pattern or the lateral position.

In the experimental verification with helium ion beams the number of irradiated points varied between 16 and 36. The relative difference between mean dose rate and $\dot{d}5-95$ value was found to increase with the number of irradiated points. This is due to the fact that the number of irradiated points is linked directly to the target size for the verification measurements performed. As the average lateral distance between the

investigated point and the beam position decreases with the target size, a reduced number of irradiated points results in a broadening of the instantaneous dose rate curve. For raster-scanned irradiations with 36, 25 and 16 spots plans the simulated $\dot{d}5-95$ values exceed the mean dose rate by 63%, 37% and 31%, respectively. For the snake-like scanning pattern there was no significant difference between the mean dose rate and $\dot{d}5-95$ value for both experiment and calculation, as high dose rate contributions occur in the beginning and end of the irradiation, making the impact of the uncertainties on the beam width model less significant. In general, to uniformize pre-clinical biological experiments in FLASH radiotherapy with raster-scanned charged particle beams, standardized and/or reported scanning patterns are needed for reproducibility of biological experiments and further modelling.

In this work we have focused on the experimental verification of the dose rate calculation framework by 2D field irradiations for a monoenergetic layer without beam modifiers. In a similar fashion to current commissioning and quality assurance procedures, dose-rate measurements of 2D or 3D irradiations could be either performed by a single detector, a block of several detectors or a 2D array detector depending on the availability of such detectors in the market. Nevertheless, with the current framework of uHDR using either transmission or ridge filter, [33]the proposed approach using a single measurement detector could be applied to validate the clinical dose engine. The proposed experimental validation along the beam axis and laterally in the high-dose region is a first step towards a more thorough treatment planning system dose-rate engine validation.

The beam intensity for uHDR irradiation at the HIT facility can fluctuate significantly within one single spill for planned particle fluences and total numbers of particles close to the achievable maximum, as can be seen in the lower part of Figure 6d. This is common for clinical synchrotron accelerators, that are operated in FLASH extraction mode at the limit of the number of the particles that can be injected within the synchrotron.[15] Since the particle spill structure is used as a starting point for the simulation, any fluctuations in the beam intensity can have a strong impact on the dose rate. This, in addition to the effects of the scanning pattern chosen, can lead to large differences between different dose rate definitions. A consensus on how the dose rate should be addressed, presented and shared among institutions is direly needed for a better understanding of in-vitro and in-vivo experiments. The presented dose rate engine could be an excellent tool to study the robustness of planned dose rates to beam intensity variations or the impact of the particle spill substructure on cell survival. Furthermore, because of its versatility, this engine could also be deployed to any particle therapy facility using active scanned beams.

5 | CONCLUSIONS

In this work, a calculation engine for raster scanned helium beam FLASH applications was developed and compared to experimental data. The presented framework provides instantaneous dose rate and cumulative dose predictions as well as 4D dose and dose rate calculations. Comparison of simulated dose rates with experimental data showed relatively good agreement using helium ion beams in uHDR mode. Further extensions and benchmarks are foreseen, allowing sound dose rate calculations for proton and carbon ion beams.

ACKNOWLEDGMENTS

This work was supported in part by NIH-1P01CA257904-01A1. This project 18HLT04 UHDpulse has received funding from the EMPIR programme co-financed by the Participating States and from the European Union's Horizon 2020 research and innovation programme.

Open access funding enabled and organized by Projekt DEAL.

CONFLICT OF INTEREST STATEMENT

Rafael Kranzer is a PTW employee while Marco Marinelli and Gianluca Verona Rinati, signed a contract with PTW-Freiburg involving financial interests deriving from the PTW diamond detectors commercialization.

DATA AVAILABILITY STATEMENT

Authors will share data upon request to the corresponding author.

REFERENCES

1. Schulz-Ertner D, Jäkel O, Schlegel W. Radiation therapy with charged particles. *Semin Radiat Oncol*. 2006;16(4):249-259. doi:10.1016/j.semradonc.2006.04.008
2. Favaudon V, Caplier L, Monceau V, et al. Ultrahigh dose rate FLASH irradiation increases the differential response between normal and tumor tissue in mice. *Sci Transl Med*. 2014;6(245):245ra93. doi:10.1126/scitranslmed.3008973
3. Montay-Gruel P, Petersson K, Jaccard M, et al. Irradiation in a flash: unique sparing of memory in mice after whole brain irradiation with dose rates above 100 Gy/s. *Radiother Oncol*. 2017;124(3):365-2369. doi:10.1016/j.radonc.2017.05.003
4. Vozenin MC, De Fornel P, Petersson K, et al. the advantage of FLASH radiotherapy confirmed in mini-pig and cat-cancer patients. *Clin Cancer Res*. 2019;25(1):35-42. doi:10.1158/1078-0432.CCR-17-3375
5. Bourhis J, Sozzi WJ, Jorge PG, et al. Treatment of a first patient with FLASH-radiotherapy. *Radiother Oncol*. 2019;139:18-222. doi:10.1016/j.radonc.2019.06.019
6. Montay-Gruel P, Bouchet A, Jaccard M, et al. X-rays can trigger the FLASH effect: ultra-high dose-rate synchrotron light source prevents normal brain injury after whole brain irradiation in mice. *Radiother Oncol*. 2018;129(3):582-2588. doi:10.1016/j.radonc.2018.08.016
7. Levy K, Natarajan S, Wang J, et al. Abdominal FLASH irradiation reduces radiation-induced gastrointestinal toxicity for the treatment of ovarian cancer in mice. *Sci Rep*. 2020;10:21600. doi:10.1038/s41598-020-78017-7

8. Diffenderfer ES, Verginadis II, Kim MM, et al. Design, implementation, and in vivo validation of a novel proton FLASH radiation therapy system. *Int J Radiat Oncol Biol Phys*. 2020;106(2):440-448. doi:10.1016/j.ijrobp.2019.10.049
9. Tessonnier T, Mein S, Walsh DWM, et al. FLASH dose rate helium ion beams: first in vitro investigations. *Int J Radiat Oncol Biol Phys*. 2021;111(4):1011-1022. doi:10.1016/j.ijrobp.2021.07.1703
10. Singers Sørensen B, Krzysztof Sitarz M, Ankjærgaard C, et al. In vivo validation and tissue sparing factor for acute damage of pencil beam scanning proton flash. *Radiother Oncol*. 2022;167:109-115. doi:10.1016/j.radonc.2021.12.022
11. Kang M, Wei S, Choi JI, Simone CB, Lin H. quantitative assessment of 3D dose rate for proton pencil beam scanning FLASH radiotherapy and its application for lung hypofractionation treatment planning. *Cancers*. 2021;13(14):3549. doi:10.3390/cancers13143549
12. van de Water S, Safai S, Schippers JM, Weber DC, Lomax AJ. Towards FLASH proton therapy: the impact of treatment planning and machine characteristics on achievable dose rates. *Acta Oncol (Madr)*. 2019;58(10):1463-1469. doi:10.1080/0284186X.2019.1627416
13. van Marlen P, Dahele M, Folkerts M, Abel E, Slotman BJ, Verbakel WFAR. Bringing FLASH to the clinic: treatment planning considerations for ultrahigh dose-rate proton beams. *Int J Radiat Oncol Biol Phys*. 2020;106(3):621-629. doi:10.1016/j.ijrobp.2019.11.011
14. Dokic I, Bojcevski J, Walsh D, et al. Carbon ion FLASH dose-rate radiotherapy: first investigation in human brain organoids. *Int J Radiat Oncol Biol Phys*. 2021;111(3):e231. doi:10.1016/j.ijrobp.2021.07.791
15. Weber UA, Scifoni E, Durante M. FLASH radiotherapy with carbon ion beams. *Med Phys*. 2022;49(3):1974-1992. doi:10.1002/mp.15135
16. Mein S, Choi K, Kopp B, et al. Fast robust dose calculation on GPU for high-precision 1H, 4He, 12C and 16O ion therapy: the FroG platform. *Sci Rep*. 2018;8:14829. doi:10.1038/s41598-018-33194-4
17. Choi K, Mein SB, Kopp B, et al. Frog-a new calculation engine for clinical investigations with proton and carbon ion beams at CNAO. *Cancers*. 2018;10(11):395. doi:10.3390/cancers10110395
18. Mein S, Dokic I, Klein C, et al. Biophysical modeling and experimental validation of relative biological effectiveness (RBE) for 4He ion beam therapy. *Radiat Oncol*. 2019;14:123. doi:10.1186/s13014-019-1295-z
19. Mairani A, Mein S, Blakely E, et al. Roadmap: helium ion therapy. *Phys Med Biol*. 2022;67:15TR02. doi:10.1088/1361-6560/ac65d3
20. Hong L, Goitein M, Bucciolini M, et al. A pencil beam algorithm for proton dose calculations. *Phys Med Biol*. 1996;41(8):1305. doi:10.1088/0031-9155/41/8/005
21. Petersson K, Adrian G, Butterworth K, McMahon SJ. A quantitative analysis of the role of oxygen tension in FLASH radiation therapy. *Int J Radiat Oncol Biol Phys*. 2020;107(3):539-547. doi:10.1016/j.ijrobp.2020.02.634
22. Vozenin MC, Hendry JH, Limoli C. biological benefits of ultra-high dose rate FLASH radiotherapy: sleeping beauty awoken. *Clin Oncol*. 2019;31(7):407-415. doi:10.1016/j.clon.2019.04.001
23. Folkerts M, Abel E, Busold S, Perez JR, Krishnamurthi V, Ling C. A framework for defining FLASH dose rate for pencil beam scanning. *Med Phys*. 2020;47(12):6396-6404. doi:10.1002/mp.14456
24. Tessonnier T, Verona-Rinati G, Rank L, Kranzer R, Mairani A, Marinelli M. Diamond detectors for dose and instantaneous dose-rate measurements for ultra-high dose-rate scanned helium ion beams. *Med Phys*. 2023. doi:10.1002/mp.16757
25. Verona Rinati G, Felici G, Galante F, et al. Application of a novel diamond detector for commissioning of FLASH radiotherapy electron beams. *Med Phys*. 2022;49(8):5513-5522. doi:10.1002/mp.15782
26. International Atomic Energy Agency. *Commissioning and quality assurance of computerized planning systems for radiation treatment of cancer, Technical Report* Series No. 430, IAEA, 2004.
27. Mein S, Klein C, Kopp B, et al. Assessment of RBE-weighted dose models for carbon ion therapy toward modernization of clinical practice at hit: in vitro, in vivo, and in patients. *Int J Radiat Oncol Biol Phys*. 2020;108(3):779-791. doi:10.1016/j.ijrobp.2020.05.041
28. Durante M, Bräuer-Krisch E, Hill M. Faster and safer? FLASH ultra-high dose rate in radiotherapy. *Br J Radiol*. 2017;91(1082):20170628. doi:10.1259/bjr.20170628
29. Rothwell B, Lowe M, Traneus E, Krieger M, Schuemann J. Treatment planning considerations for the development of FLASH proton therapy. *Radiother Oncol*. 2022;175:222-230. doi:10.1016/j.radonc.2022.08.003
30. Schwarz M, Traneus E, Safai S, Kolano A, van de Water S. Treatment planning for Flash radiotherapy: general aspects and applications to proton beams. *Med Phys*. 2022;49(4):2861-2874. doi:10.1002/mp.15579
31. Gao H, Liu J, Lin Y, et al. Simultaneous dose and dose rate optimization (SDDRO) of the FLASH effect for pencil-beam scanning proton therapy. *Med Phys*. 2022;49(3):2014-2025. doi:10.1002/mp.15356
32. Ramesh P, Gu W, Ruan D, Sheng K. Dose and dose rate objectives in Bragg peak and shoot-through beam orientation optimization for FLASH proton therapy. *Med Phys*. 2022;49(12):7826-7837. doi:10.1002/mp.16009. [published online October 12, 2022.
33. Liu R, Charyyev S, Wahl N, et al. An integrated physical optimization framework for proton stereotactic body radiation therapy FLASH treatment planning allows dose, dose rate, and linear energy transfer optimization using patient-specific ridge filters. *Int J Radiat Oncol Biol Phys*. 2023;116(4):949-959. doi:10.1016/j.ijrobp.2023.01.048

How to cite this article: Rank L, Dogan O, Kopp B, et al. Development and benchmarking of a dose rate engine for raster-scanned FLASH helium ions. *Med Phys*. 2024;51:2251–2262. https://doi.org/10.1002/mp.16793